arXiv:1611.01266v1 [astro-ph.HE] 4 Nov 2016

Estimation of Mass of Compact Object in H 1743-322 from 2010 and 2011 Outbursts using TCAF Solution and Spectral Index - QPO Frequency Correlation

Aslam Ali Molla[1], Sandip K. Chakrabarti[2,1], Dipak Debnath[1], Santanu Mondal[3,1]
aslam@csp.res.in; chakraba@bose.res.in; dipak@csp.res.in; santanu@csp.res.in

ABSTRACT

The well known black hole candidate H 1743-322 exhibited temporal and spectral variabilities during several outbursts. Daily variation of the accretion rates and the flow geometry change on a daily basis during each of the outbursts could be understood very well using the recent implementation of two component advective flow (TCAF) solution of the viscous transonic flow equations as an additive table model in XSPEC. This has dramatically improved our understanding about the accretion flow dynamics. Most interestingly, the solution allows to treat mass of the black hole candidate as a free parameter and there mass could be estimated from spectral fits. In this paper, we fit the data of two successive outbursts of H 1743-322 in 2010 and 2011 and studied evolutions of accretion flow parameters, such as, two component (Keplerian and sub-Keplerian) accretion rates, shock location (i.e., size of the Compton cloud), etc. We assume that the model Normalization remains the same accross the states in both these outbursts. We use this to estimate mass of the black hole and found that it comes out in the range of $9.25 - 12.86 M_{\odot}$. For the sake of comparison, we also estimated mass using Photon index vs. QPO frequency correlation method which turns out to be $11.65 \pm 0.67 M_{\odot}$ using GRO J1655-40 as reference source. Combining these two estimates, the most probable mass of the compact object becomes $11.21^{+1.65}_{-1.96} M_{\odot}$.

Subject headings: X-Rays:binaries – stars individual: (H 1743-322) – stars:black holes – accretion, accretion disks – shock waves – radiation:dynamics

1. Introduction

In the last two decades, specially after the launch of *Rossi X-Ray Timing Explorer (RXTE)*, our understanding about the accretion process around a black hole candidate (BHC) is significantly improved. They are only detectable when matter from a companion, be it from the Roche lobe or from its winds accretes on them. Radiations are emitted in this process allowing them to infer on the accretion process. It is even better, when the rate of accretion changes rapidly, since the object can then go through various spectral states in quick successions and the timing properties also give out information about the companion. Normally, an outbursting BHC shows four different spectral states, namely, hard (HS), hard-intermediate (HIMS), soft-intermediate (SIMS), and soft (SS) (Belloni et al. 2005; McClintock & Remillard 2006; Nandi et al. 2012; Debnath et al. 2013). Low frequency Quasi Periodic Oscillations (QPOs) in some of these states are also observed (e.g., Remillard & McClintock 2006). Evolution of temporal and spectral properties of several BHCs have been studied by many workers during their outbursts (e.g., Belloni et al., 2005; McClintock & Remillard, 2006; Nandi et al., 2012) and it has been noted by several authors that different spectral states are related to different branches of hardness intensity diagram (HID; Belloni et al. 2005; Debnath et al. 2008) or accretion rate ratio intensity diagram (ARRID; Jana et al. 2016).

[1]Indian Center for Space Physics, 43 Chalantika, Garia St. Rd., Kolkata, 700084, India.

[2]S. N. Bose National Centre for Basic Sciences, Salt Lake, Kolkata, 700098, India.

[3]Instituto de Física y Astronomía, Facultad de Ciencias, Universidad de Valparaíso, Gran Bretana N 1111, Playa Ancha, Valparaso, Chile

It is well known that in order to explain majority of the black hole spectra one needs two types of components: one is a multi-color blackbody component radiated by the standard Keplerian disk (Shakura & Sunyaev 1973) and the other is a power-law (PL) component, originated from a so-called "Compton cloud" (Sunyaev & Titarchuk 1980, 1985). There are several models which describe the nature and origin of this "Compton cloud". These range from a magnetic corona (Galeev et al. 1979) to a hot gas corona over the disk (Haardt & Maraschi 1993; Zdziarski et al. 2003). Chakrabarti & Titarchuk (1995; hereafter CT95), even before the launch of RXTE, considered the well known component solution of transonic flows (see, Chakrabarti 1990; Chakrabarti 1996), namely, the CENtrifugal Pressure supported BOundary Layer (CENBOL) to represent the "Compton cloud" in their Two Component Advective Flow (TCAF) solution. From the observational evidence it is now established that, both the components are dynamic and the low angular momentum halo component (which does not require viscosity to accrete) is moving faster than the more viscous Keplerian disk (Soria et al. 2001; Smith et al. 2002; Wu et al. 2002; Cambier & Smith 2013; Tomsick et al. 2014). In the early stage of an outburst, the gravitational energy is mostly stored in the advective component as thermal energy and as the day progresses, this energy is released gradually by inverse Comptonization since the soft (seed) photon flux also rises. In the declining phase the process is reversed, though the time scale varies. Thus the hot post-shock flow in HS becomes cooler progressively in HIMS, SIMS and SS. Whether or not all the states would be visited will depend on the how long the supply of viscous accretion creating the Keplerian disk lasts. In a transonic flow with low enough viscosity, the centrifugal pressure slows down the flow and a standing or oscillating shock would be formed depending on whether the Rankine-Hugoniot conditions are satisfied (Chakrabarti 1989, 1996) or not. This centrifugal barrier region is puffed up and acts as the "Compton cloud". Recently, self-consistency and stability check (Giri & Chakrabarti 2013; Mondal & Chakrabarti 2013) of the transonic solution have been made which support from both the hydrodynamic and radiative points of view that an advective flow will desegregate into a TCAF solution (CT95) when viscous stress near the equatorial plane is very high.

Successful fits of data from several black hole candidates have been recently obtained and the general nature of the accretion flow dynamics has been understood (Debnath, Chakrabarti & Mondal 2014; Mondal, Debnath & Chakrabarti 2014; Debnath, Mondal & Chakrabarti 2015a; Debnath, Molla, Chakrabarti & Mondal 2015b; Jana et al. 2016; Molla et al. 2016; Chatterjee et al. 2016; Mondal, Chakrabarti & Debnath 2016). Physical flow parameters such as the two types of accretion rates (disk and halo), shock location (size of the Compton cloud), shock strength and the mass of the black hole were obtained after the inclusion of TCAF solution (CT95, Chakrabarti 1997) as an additive table model in HEASARC's spectral analysis software package XSPEC.

The black hole candidate H 1743-322 is very active as it displayed several X-ray outbursts since its first detection in 1977 August-September by the *Ariel V* all sky monitor (Kaluzeinski & Holt 1997) and *HEAO I* satellite (Doxsey et al. 1977). After its first detection, it went to the quiescent state and remained that way for a long time till 1984. A couple of X-ray activities were reported by *EXOSAT* observations in 1984 (Raynolds 1999) and by TTM/COMIS instruments on board *Mir-Kvant* in 1996 (Emelyanov et al., 2000). During the scanning of the galactic center on March 21, 2003, *INTEGRAL* detected a bright source named IGR J17464-3213 (Revnivtsev et al. 2003) which turned out to be H 1743-322 (Markwardt & Swank 2003). Since then, it exhibited several X-ray activities with regular intervals of one or two years. This active low mass X-ray binary source is located at the sky location of R.A. = $17^h46^m15^s.61$, Dec = $-32^\circ14'00''.6$ (Gursky et al., 1978). Mass of this BHC has not been dynamically measured yet, although Petri (2008), with their high frequency QPO model estimated that its mass could be between $9M_\odot$ and $13M_\odot$. From the correlation between spectral and timing properties of black holes, Shaposhnikov and Titarchuk (2009; hereafter ST09) calculated mass of this black hole candidate to be $13.3 \pm 3.2\ M_\odot$ using 2003 data of RXTE PCA by taking GX 339-4 as a reference source of known mass. The inclination angle was reported to be about $\theta = 75^\circ \pm 3^\circ$ (McClintock et al. 2009). The source is located at a distance of 8.5 ± 0.8 kpc with an angle of inclination and spin of $-0.3 < a < 0.7$, with a 90% confidence (Steiner et al. 2012).

It is well known that timing and spectral properties of a BH are tightly correlated. Titarchuk & Fiorito (2004), introduces a useful tool to determine mass of stellar massive black hole as well as super massive black hole by the correlation between power-law (PL)

photon indices and characteristic frequencies of the observed quasi-periodic oscillation. Shaposhnikov & Titarchuk (2007; hereafter ST07) employed this idea to estimate the mass of Cyg X-1 and obtained the mass to be $M_{CygX-1} = 8.7 \pm 0.8 M_{\odot}$. This method was also used by Fiorito & Titarchuk (2004), Dewangan, Titarchuk & Griffiths (2006) and Strohmayer et al. (2007), Titarchuk & Seifina (2016a,b) to estimate masses of a number of ultra-luminous X-ray sources. This idea was applied successfully to calculate mass of an AGN Mrk 766 by Giacche et al. (2014) to obtain $M_{BH} = 1.26^{+1.00}_{-0.77} \times 10^6 M_{\odot}$. Papadakis et al. (2009) and Sobolewska & Papadakis (2009) have applied this method to estimate the mass of 14 AGNs. Using a simplified accretion disk model of non-interacting particles, Petri (2008) also presented a way to estimate the mass and spin of BHCs. However, this method required another reference source to estimate the mass. Furthermore, the error-bar obtained by ST09 on estimated mass of H 1743-322 is also quite large. Most importantly, since 2003 outburst of H 1743-322 is quite anomalously bright with other effects such as activities in radio, which means the jets could also contribute to X-rays, it was essential to apply this method to a more 'normal' outburst event which occured more recently. This motivated us to estimate the mass once more using more recent outbursts.

In, 2010 and 2011, H 1743-322 exhibited two X-ray flaring activities (Yamaoka et al. 2010; Kuulkers et al. 2011) with the same type of state transition characteristics (Debnath et al. 2013) as reported in other outbursting sources (Debnath et al. 2008, 2015a,b; Jana et al. 2016, Chatterjee et al. 2016 and references therein). Both the outbursts were covered by *RXTE* almost on a daily basis for around two months during the outbursts. Study of gross aspects of the temporal and spectral properties during these two outbursts using *RXTE PCA* data with combined disk black body (DBB) and power law (PL) model has already been made by Debnath et al. (2013). Study of spectral property using *RXTE PCA* data during its 2010 outburst with *TCAF* solution has also been done quite recently by Mondal et al. (2014), where TCAF model fitted normalization (N) was allowed to vary for the best fit. In the present paper, we restrict the normalization N within a narrow range to estimate the mass of the central object independently from two successive outbursts (2010 and 2011) of H 1743-322, in order to investigate if there are still consistent fits from the TCAF solution. This would indicate that no free parameter other than those five (mass, two accretion rates, shock location and shock compression ratio) required by TCAF is necessary to explain the entire outburst. N would otherwise be expected to remain constant as it is an intrinsic property of the system from one outburst to another, though it could have an error-bar consistent with the error-bars of other parameters on which it depends, such as the mass, distance and the inclination angle. Systematic deviation of N from a constant value could be due to several effects such as the precession in the disk occurs which changes the projected surface area of emission. Significant fluctuations in N could be interpreted as contributions of X-rays from jets or outflows which have not been included in this version of TCAF model *fits* file.

In Molla et al. (2016), Jana et al. (2016) and Chatterjee (2016), we successfully applied this constant normalization method to estimate masses of three MAXI transient compact objects, such as, MAXI J1659-152, MAXI 1836-194, and MAXI J1543-564 respectively. In Molla et al. (2016), we also verified estimated mass of MAXI J1659-152 from that obtained by us using propagating oscillatory shock (POS) model (Chakrabarti et al. 2005, 2008; Debnath et al. 2010, 2013). The successful interpretation of masses of these MAXI objects also motivated us to estimate mass of the well known transient BHC H 1743-322 using the same method.

The organization of this *paper* is the following: in the next Section, we discuss observation and data analysis procedures. In §3, we present results of TCAF model fitted spectral analysis. From this we estimate the mass of the object. We also compare with the mass obtained from ST09. In the final Section, we present a brief discussion and draw concluding remarks.

2. Observation and Data Analysis

We take RXTE/PCA science data from NASA data archive for analysis. We choose the data produced in 2010 and 2011 by RXTE as in this period H 1743-322 show spectral and timing property very clearly almost on a daily basis. We analyze the data of 26 observational IDs for 2010 outburst starting from 2010 August 9 (MJD=55417) to 2010 September 30 (MJD=55469) and the data of 27 observational IDs for 2011 outburst starting from 2011 April 12 (MJD=55663) to 2011 May 19 (MJD=55700). In our data analysis we exclude the data taken for elevation angles less than 10°, for offset greater than 0.02° and those acquired dur-

ing the South Atlantic Anomaly (SAA) passage. We use HEASARC's software package HeaSoft version HEADAS 6.15 and XSPEC version 12.8 to carry out our timing and spectral data analysis procedure.

2.1. Timing Analysis

In order to observe timing property of RXTE/PCA data we use "binned mode" data which was available for 0-35 channels only, with a maximum time resolution of 125 μs. For the timing analysis of PCA data we restrict ourselves in the energy range of $\sim 2-15$ keV. After extracting the light curve, Power Density Spectrum (PDS) is generated by the standard FTOOLS task "powspec" with a suitable normalization. We find that the power beyond 50 Hz frequency is insignificant so we rebinned the data to have 0.01s time resolution to obtain the Nyquest frequency of 50 Hz and also to get the *QPO* frequency. In Figure 1, we show the PDS with a QPO having primary frequency of 1.008 ± 0.003 Hz and the total exposure time of data is 3379s.

2.2. Spectral Analysis

In order to carry out the spectral analysis of the PCA data, we use "standard2" mode Science Data (FS4a*.gz) in the energy range 2.5-25. keV with a time resolution of 16 sec. We extract spectra from all the layers of PCU2 for 128 channels (without any binning/grouping the channels). We generate source spectrum using FTOOLS task "SEEXTRCT" with 16 sec time bin from "standard2" science even mode data. In order to produce background *fits* file we use FTOOLS task "runpcabackest" with the standard FILTER file provided with the package. To generate background source spectrum we again use FTOOLS task "SEEXTRCT" with 16 sec time bin from background fits file. The "pcarsp" task is used to produce the response file with appropriate detector information. To fit the spectra we use TCAF based model *fits* file. In order to achieve the best fit, we use Gaussian line of peak energies around 6.5 keV and around 3.8 keV for both the outbursts. Spectral data is fitted with model composition wabs×(TCAF+Gaussian+Gaussian). The hydrogen column density (N_H) obtained for this source was 1.6×10^{21} atoms cm^{-2} (Capitanio et al., 2009) from Swift/XRT observations, which was lower energy range than that for RXTE/PCA and therefore we keep it fixed for both 2010 and 2011 outburst for absorption model *wabs*. We also use a fixed 0.5% systematic instrumental error. We use "err" command to find out 90% confidence error values in model fitted parameters. During a spectral fit, using the TCAF based fits file, we supply five model input parameters: *i*) black hole mass (M_{BH}) in solar mass ($M_\odot$) unit, *ii*) sub-Keplerian rate ($\dot{m}_h$ in $\dot{M}_{Edd}$), *iii*) Keplerian rate ($\dot{m}_d$ in Eddington rate $\dot{M}_{Edd}$), *iv*) location of the shock (X_s in Schwarzschild radius r_g=$2GM/c^2$), *v*) compression ratio (R) of the shock. To fit a black hole spectrum with the TCAF in XSPEC, we generated model *fits* file (here *TCAF0.3.fits* was used). For this, we use theoretical spectra generating software and vary our basic five input parameters in suitably generalized CT95 code and then include it in XSPEC as a local additive model. During the analysis of both the outbursts we keep all the parameters free, except with the restriction that the N which comes of the fit must be in a narrow range, i.e., a constant with a small enough error bar. In order to extract photon index from spectral data, we refit entire 2010 and 2011 outburst data sets using CompTB model (Farinelli et al. 2008) with spectral fitting model composition as wabs×(CompTB+Gaussian).

3. Results

Here we present results based on spectral analysis using TCAF *fits* file. Classification of different spectral states and their transitions during both 2010 and 2011 outbursts of H 1743-322 are done on the basis of the values of flow parameters extracted from TCAF *fits*, and values of the "QPO frequency". These classifications are consistent with Debnath et al. (2013).

3.1. Spectral Data Fitted by TCAF model

In Figs. 2 & 4, we show variation of background subtracted *RXTE* PCA count rate in the energy range of 2-25 keV (0-58 channels) and QPO frequency along with model fitted parameters during the 2010 and 2011 outbursts. From TCAF *fits* we extract physical parameters such as the disk rate ($\dot{m}_d$), the halo rate ($\dot{m}_h$), the location of shock (X_s) representing the size of the Compton cloud, and the compression ratio (R). Variations of these derived parameters are shown in Figs. 2(b-e) & 4(b-e). During both the outbursts, we fit 2.5-25 keV PCA spectral data with TCAF solution by leaving all the parameters free. From the fit, we get the variation of model normalization and mass. By restricting the model normalization in a narrow range allowed by our criteria of acceptable fit ($\chi^2_{red} < 2.0$), we obtain the mass range to be $9.51M_\odot$ - $12.42M_\odot$ for

2010 outburst and $9.43M_{\odot}$ - $12.71M_{\odot}$ for 2011 outburst. In Figs. 3 & 5, we show variation of model normalization and derived mass of the BHC H 1743-322 using these respective data. Variation of normalization and mass are shown in Figs. 3 (a) & (b) for the 2010 outburst and in Figs. 5 (a) & (b) for the 2011 outburst. As a cross check, we repeat the fitting procedure by keeping model normalization fixed to a value of 15.55, which is the averaged value of model normalizations obtained from the fits above and we obtain a variation of mass to be in the range of $9.63M_{\odot}$ - $12.34M_{\odot}$ for 2010 outburst and $9.25M_{\odot}$ - $12.86M_{\odot}$ for 2011 outburst. The plots are shown in Figs. 3 (c) and 5 (c). Depending on the extracted accretion flow parameters and nature of QPOs (shape, frequency, Q-values, rms), we identify four spectral states, namely, HS, HIMS, SIMS, and SS. We observe that the transitions (marked with vertical dashed lines in Fig. 2) occur almost on the same date for 2010 outburst (as reported in Mondal et al. 2014, 2015) where the same data was fitted by TCAF keeping mass as a constant parameter (11.4 $M_{\odot}$) and using free normalization constant during the whole outburst. TCAF model fitted unfolded spectra are shown in Fig. 6 from HS and SS. The possible reason of double Gaussian is discussed later. In Debnath et al. (2013) spectral classification was made on the basis of the variation of DBB and PL model fitted fluxes and properties of QPOs. During the 2011 outburst, the spectral transition dates do not exactly match with the transition dates as reported in Debnath et al. (2013). In Appendix Table I, II, III & IV these fitted and derived parameters are presented with parameter error values. The evolution of the spectral states, observed QPO frequencies and variation of model normalization values and mass of the black hole obtained from each observation during 2010 & 2011 outbursts are also given in the tables. As a cross check, we find that if we freeze all the model parameters to the values obtained from their best fit and try to see the variation of χ^2_{red} by only changing its mass, then we see that value of $\chi^2_{red} \geq 2$ when the mass of the black hole is chosen outside the range of $9M_{\odot} - 13M_{\odot}$. All these results are shown in Figs. 7 & 8. We also measured mass of the source using ST07 photon index - QPO Freq. correlation method (see, Fig. 9), which is initially refereed as a BH scaling method (Fiorito & Titarchuk 2004; ST07). The estimated mass ($=11.65 \pm 0.67M_{\odot}$) from this method is well within TCAF model fitted mass range.

3.2. Spectral evolution during 2010 and 2011 Outburst

Detailed study of temporal and spectral evolution of this source during 2010 & 2011 outburst with DBB-PL model (Debnath et al., 2013) and spectral evolution of 2010 outburst with TCAF solution (Mondal et al., 2014) has already been done. The analysis indicates transition of spectral states and a clearer picture of accretion flow dynamics emerged. However, since the mass of the object was not known dynamically, a suitable value of the mass was chosen and the normalization factor was allowed to vary for an acceptable fit. In the present paper, on the other hand, we concentrate on the determination of mass by restricting the normalization to be in the narrowest possible range, as allowed by acceptable range of $\chi^2_{red} < 2.0$. This is because the normalization in TCAF is a function of the mass, distance, and the inclination angle only, after the data is corrected due to the instrumental response and the absorption. This gives a narrow range on the mass. After obtaining the fit for the 2010 outburst, we fit the 2011 outburst also for the same normalization factor range. This is to find out if the same normalization factor also yields a similar mass as obtained in 2010 outburst.

(i) Hard-State in the Rising phase: In hard state, the spectrum is dominated by hard photons. The source remains in this state for the initial 3 days of the outburst (from MJD = 55417.29 to 55419.11) in 2010, and for 6 days of the outburst (from MJD=55663.68 to 55668.48) in 2011 with very low disk rate and comparatively high halo rate. Changes in the shock location, compression ratio as well as the QPO frequency are slow (see, Fig. 2 and 4). We define third day of observation (MJD =55420.3) for 2010 outburst and fifth day of observation (MJD=55667) for 2011 outburst as the transition day from HS to HIMS since on the transition day value of halo rate for both the outbursts has attained its maximum value in the rising phase and after this day disk rate increases very rapidly (0.011 to 0.039 for 2010 and 0.013 to 0.075 for 2011), and the location of the shock as well as the compression ratio decreases very rapidly for both the outbursts. QPO frequency changes very rapidly for both the outbursts (1.045Hz to 1.174Hz for 2010 and 0.885Hz to 1.364Hz for 2011 outburst).

(ii) Hard-Intermediate State in Rising phase: The source remains in this state for the next four days in 2010 and for the next six days in 2011 until the next transition occurred on MJD =55424.1 during 2010

and MJD=55672.9 during 2011 outburst. During this period the spectrum becomes somewhat softer which is reflected in the increased value of Keplerian rate (0.039 to 1.008 $\dot{M}_{Edd}$ for 2010 and 0.075 to 0.286 $\dot{M}_{Edd}$ for 2011). During this phase, the shock moves closer to the black hole and became weaker ($R \sim 1.981$ to 1.075 for 2010 and $R \sim 1.754$ to 1.076 for 2011). This is because the post-shock region which acts as the Compton cloud is cooled down by increasing number of seed (soft) photons. QPO frequency increases monotonically and reaches to its maximum value indicating an end of this phase.

(iii) Soft-Intermediate State in Rising phase: The spectrum makes a transition from HIMS to SIMS when the resonance nature of QPO frequency (Molteni et al. 1996, hereafter MSC96; Chakrabarti et al. 2015, hereafter CMD15) breaks down for both the outbursts and the value of disk rate further increased by causing the spectrum more soft. The source remains in this state for a very short period about 1 day in 2010 and about 3.5 days in 2011. In this state, the spectrum becomes softer causing an increase in the Keplerian rate and decrease in the sub-Keplerian rate although on MJD = 55674.3 halo rate is very high (0.794 M_{Edd}) it may be due to high photon count on that day (see top panel of Fig. 4). Increase in the disk rate cools down the post shock region very rapidly, so the shock location and its strength decreases very sharply. In this state LFQPO occurs sporadically as the shock itself may not form and the centrifugal barrier oscillates (Debnath et al, 2013). This is the common feature of soft intermediate state.

(iv) Soft State: After the completion of the soft intermediate state, the source enters into the soft state with a high Keplerian rate and very low sub-Keplerian rate. The shock location and the shock strength remain almost constant. The source remains in this state for 24 days (MJD= 55425.2 to 55448.8) in 2010 outburst and for about 9.5 days (MJD= 55678.1 to 55687.6) in 2011 outburst. No sign of QPOs in this period in both the outbursts as the cooling time scale is very short and the resonance condition cannot be satisfied.

(v) Soft-Intermediate State in Declining phase: The source enters in this state with when sporadic QPOs start and remains in this state for almost ~ 4 days (MJD = 55450.3 to 55453.7) and for 2.5 days (MJD=55687.6 to MJD=55690.1) respectively for 2010 and 2011 outbursts. In 2010 outburst, it has shown a sporadic QPO with the peak frequency of 2.489 ± 0.018Hz whereas in 2011 outburst it has shown only one sporadic QPO with a frequency of 2.215 ± 0.021Hz. In this state, the total PCA rate as well as the total flow rate ($\dot{m}_d + \dot{m}_h$) are nearly constant for both the outbursts. After this state, on MJD = 55455.4 and on MJD = 55690.1, a QPO was observed with a much higher frequency of 6.417 ± 0.252 Hz (2010 outburst) and 2.936 ± 0.024 Hz (2011 outburst) than its previous day. This is clearly an indication of the beginning of the declining HIMS.

(vi) Hard-Intermediate State in Declining phase: In both the outbursts, the source enters in this state right after the occurrences of the maximum value of QPO frequency and remains in this state showing a prominent Type C QPO almost on a daily basis. In this phase, the disk rate drops rapidly and the shock moves away from the black hole, thereby increasing the size of the Compton cloud. Due to lower cooling, the strength of the shock also increases. Due to reduction of viscosity at the outer disk, which causes the initiation of the declining state, the Keplerian rate continues to decrease and the halo rate increases (Fig. 2c, Appendix Table I for 2010 and Fig. 4c, Appendix Table II for 2011). The spectrum makes a transition on MJD = 55462.6 for 2010 and on MJD = 55695.4 for 2011 from the HIMS to the HS showing a sudden jump in halo rate. The observed halo rate is found to be maximum due to a sudden rise in the location and the strength of the shock.

(vii) Hard State in Declining phase: This state starts with a high halo rate in both the outbursts and continued from MJD = 55462.6 and from MJD = 55695.4 for 2010 and 2011 outburst till end of the observation. During this period, the Keplerian rate is very low with a comparatively higher halo rate. The shock moves away with increasing strength (see Fig. 2, Fig. 4 and Appendix Table I, Appendix Table II). QPO was observed till the last date (0.74 Hz to 79 mHz in 2010 and 1.186 Hz to 0.382 Hz in 2011).

3.3. Mass Estimation using TCAF solution

We applied Molla et al. (2016), constant TCAF model normalization method to estimate mass of the source by analyzing 2010 and 2011 outbursts of H 1743-322. According to TCAF solution, model normalization (N) should not vary significantly on a daily basis of a particular BH binary system, since it depends on physical intrinsic parameters, such as, mass, distance, disk inclination angle etc. So, we applied this concept to estimate mass of the BHC H 1743-322 by combined spectral analysis of the source during its two

successive outbursts 2010 and 2011 using RXTE/PCA data. We first fitted the spectra using current version of the TCAF solution by keeping all model parameters as free. Interestingly, obtained model normalization values comes within a narrow range for both the outbursts across all the spectral states. During 2010 outburst N is found within 9.79 – 27.36, and for 2011 outburst, it is found in between 10.01 – 16.18. Since, in TCAF solution, mass is an independent parameter, we obtained mass range of the source as $9.51M_{\odot} - 12.42M_{\odot}$ for 2010 outburst and $9.43M_{\odot} - 12.71M_{\odot}$ for 2011 outburst. We then refitted all the spectra using constant normalization value N=15.55 (obtained by taking average of the free model normalization values of both outbursts) and we obtained mass range of the source as $9.63M_{\odot}$ to $12.34M_{\odot}$ (for 2010 outburst), and $9.25M_{\odot}$ to $12.86M_{\odot}$ (for 2011 outburst). Now, by combining the results of 2010 & 2011 outbursts, the mass of the black hole candidate source can be constrained within a range of $9.25M_{\odot}$ to $12.86M_{\odot}$. To verify this estimated mass range of the source, we refit all spectra by freezing all the model parameters. Mass of the BH was changed in $9M_{\odot} - 13M_{\odot}$ range to observe variation of χ^2_{red}. We also restrict ourself $\chi^2_{red} \leq 2$ for best fits. The parabolic variations of the χ^2_{red} (as shown in Fig. 7 & 8) for all spectra show minima in between $\sim 10.6M_{\odot} - 11.6M_{\odot}$.

3.4. Mass Estimation using Photon Index (Γ) - QPO frequency (ν) Correlation Method

Titarchuk & Fiorito (2004) introduced a model to correlate between spectral fitted photon index (Γ) and the observed QPO frequency (ν). This method is used to estimate mass of a few BHCs (ST07). In this model, the central source is surrounded by a 'Compton cloud' along with a transition layer between this Compton cloud and Keplerian disk. According to this model the change in QPO frequency explained as the magneto-acoustic resonance oscillation frequency of the bounded transition layer (Titarchuk & Wood, 2002) and the photon index (due to change in optical depth of the hot electrons) of emitted spectrum is due to change in the size of Compton cloud. In the TCAF paradigm (Chakrabarti & Titarchuk, 1995) this Compton cloud is the post-shock region of the accretion disk and the oscillation occurs due to near equality of Compton cooling time scale and the infall time scale (MSC96; CMD15). The change in QPO frequency and the photon index is also demonstrated in TCAF solution (Chakrabarti et al. 2008; Nandi et al. 2012; Debnath et al. 2014). The empirical relation given in ST07 by,

$$\Gamma(\nu) = A - DBln[exp(\frac{\nu_{tr} - \nu}{D}) + 1] \qquad (1)$$

where A is the saturation point of photon index, B is the slope of QPO - PL index curve which scales the mass and ν_{tr} is the transition/threshold frequency above which the saturation of Γ happens. Value of D controls how fast the transition occurs. In order to find mass of an unknown source BH, this method requires another source of known mass BH with similar type of correlation curve as a reference.We consider the 2005 outburst data of GRO J1655-40 as the reference source for scaling of PL index - QPO frequency correlations to estimate BH mass in H 1743-322, because photon indices for these two objects demonstrate the same saturation level (see Fig.9). Note, this is necessary condition for applicability of scaling technique (see details in Sec. 7.3 of Seifina et al. 2014). This outburst data was also used by ST07 to calculate mass of Cyg X-1 and use the same values of A, B, D and ν_{tr} as used by ST07 to fit the data of GRO J1655-40. In order to study the correlation between QPO and PL-index we extract PL index using CompTB model (Farinelli et al. 2008) and we found that the value of PL index obtained from CompTB model is slightly higher due to bulk motion Comptonization effect which hardens the spectrum a little bit than the PL index obtained from DBB - PL model, this difference in PL index would cause the difference in the value of mass of central object. During the fitting we freeze D = 1.0 as in ST07. We use 2005 outburst data of GRO J1655 - 40 and use the fitted values of $A_{J1655} = 2.28 \pm 0.07$, $B_{J1655} = 0.13 \pm 0.02 Hz^{-1}$ and $\nu_{tr,J1655} = 6.64 \pm 0.51 Hz$ as used in ST07 paper. The best fitted curve is shown by solid blue (online) curve in Fig. 9. The best fitted value for H 1743-322 is $A_{H1743} = 2.23 \pm 0.05$, $B_{H1743} = 0.246 \pm 0.035 Hz^{-1}$ and $\nu_{tr,H1743} = 2.95 \pm 0.58 Hz$. The best fitted curve is shown by solid red (online) line in Fig. 9. In this figure monotonical growth and elongated part with index saturation (constancy) on the level of Γ = 2.23 are well seen. The index revealed in H1743-322 based on 2010 and 2011 data is similar to those established in a number of other black hole candidates and has been considered to be an observational evidence for the presence of a black hole in this source (see, ST07, ST09 and references therein). Applying ST07 method for BH source H 1743-322 by taking GRO J1655-40 as a reference source of mass $6.3 \pm 0.5 M_{\odot}$ (Greene et al. 2001)

we obtain mass of this BH source as,

$$M_{H1743} = B_{H1743}\frac{M_{J1655}}{B_{J1655}} = 11.65 \pm 0.67 M_{\odot}$$

which is in the same ball park as in our result.

4. Discussions and Concluding Remarks

In this paper we estimated the mass of the black hole candidate H 1743-332 by using two independent methods. First, we investigate the evolution of spectral properties of Galactic transient black hole candidate H 1743-322 during its 2010 & 2011 outbursts keeping the normalization as a constant parameter. We extract mass of the central object independently from each observation as was done in Molla et al. (2016). We use the TCAF solution after its inclusion as a local additive table model in HEARSRC's spectral analysis software package XSPEC. Depending on the extracted flow parameters and nature of QPOs, similar to Debnath et al. (2013), we also observe four spectral states, such as, hard, hard-intermediate, soft-intermediate and soft during both the 2010 & 2011 outbursts of H 1743-322. In the process of fitting, we found that the model normalization remains within a narrowest possible range for acceptable fits. Most importantly, we also found that the same average normalization obtained from the 2010 outburst fits the data of 2011 outburst equally well. In order to obtain a rough estimation of the variation of thermal (DBB) and non-thermal (PL) fluxes during the outbursts, we follow the procedure given in Debnath et al. (2013) and see that QPO is totally absent in soft states for both the outbursts as in 2003 outburst of H 1743-322 (McClintock et al., 2009; ST09). It is to be noted that low frequency QPOs are thought to be due to shock oscillation phenomenon in the TCAF paradigm. Shocks oscillate when the cooling time scale roughly matches with the infall time scale (MSC96; CMD15) inside CENBOL. Oscillating shock intercepts oscillating number of soft photons and hard photons are emitted accordingly, causing QPOs (Chakrabarti & Manickam, 2000).

In order to keep the normalization constant or nearly constant, for a better fit, sometimes we require two Gaussian curves whose peaks are found to be at around 3.8 keV and 6.5 keV (see, dotted curves in Figs. 6b, 6d and short dashed curves in Figs. 6a, 6c). We interpret 6.5 keV line as the iron-line emitted from the Keplerian disk. However, the peak around 3.8 keV line is clearly not the red-shifted component of the iron line, because it is much stronger than the 6.5 keV line. Moreover, it is only about one-fifth of the continuum photon flux. The only explanation of this component must be that it is the signature of reappearance of the inner Keplerian disk as the soft-state is approached. Indeed, it can be seen from the Appendix Tables I and II that the normalization of this component is rising as one goes from the harder state to the softer state and is going down again in the declining phase. In any case, since the pressure and therefore shear is higher at the inner edge, the angular momentum transport is fastest (Chakrabarti & Molteni, 1995) and the reappearance of the Keplerian disk in softer states must commence from the inner disk. So our work possible points to this aspect very clearly.

Spectral analysis of 2010 outburst of this source with TCAF model has been done by Mondal et al. (2014) assuming a fixed mass of the black hole ($11.4 M_{\odot}$) and keeping the model normalization free. On the other hand, to determine the mass independently, we fitted all the spectra using all TCAF model parameters as free and for both outbursts, we observe a narrow variation of model normalization (9.79 – 27.36 for 2010 outburst and 10.01 – 16.18 for 2011 outburst). Mass of the source is obtained in the range: $9.51 M_{\odot} - 12.42 M_{\odot}$ (for 2010 outburst) and $9.43 M_{\odot} - 12.71 M_{\odot}$ (for 2011 outburst). We then refitted all the spectra using constant average normalization value of $N = 15.55$ and obtained the mass from $9.63 M_{\odot}$ to $12.34 M_{\odot}$ (for 2010 outburst), and $9.25 M_{\odot}$ to $12.86 M_{\odot}$ (for 2011 outburst). We then computed variation of χ^2_{red} with mass in this general range of $9 - 13 M_{\odot}$ and found that χ^2_{red} is minimum in between $\sim 10.6 M_{\odot} - 11.6 M_{\odot}$. To compare, we also estimate the mass of the source using another independent method, i.e., ST07 photon index (Γ) vs. QPO frequency correlation scaling) by taking data of the both 2010 and 2011 outbursts of H 1743-322. Our estimated mass from this method is $11.65 \pm 0.67 M_{\odot}$, which was obtained by using GRO J1655-40 as a reference source. Combining both the TCAF and the ST07 methods, we believe that the mass of H 1743-322 should be in the range of $11.21^{+1.65}_{-1.96} M_{\odot}$. We find that the TCAF result gives the mean mass to be slightly lower as compared to the mean mass from ST09.

TCAF represents a comprehensive solution of equations governing the flow. It attempts to explain the spectral and timing properties simultaneously and extract physical parameters such as the accretion rates, size of the Compton cloud and even the Mass of the

central object. Each individual observation gives a new and independent mass estimate. This is in contrast with the method of ST07 and ST09 where a refereence source is also required. So far, the effects of the magnetic field and spin have not been included in TCAF. However, since shocks are located far away in harder states, effects of spin would not be significant on the mass obtained from harder states. Nevertheless, we are incorporating these effects and the results would be published elsewhere.

Acknowledgments

A.A.M. and S.M. acknowledge supports from MoES sponsored senior and post-doctoral research fellowships respectively. D.D. acknowledges support from project fund of DST sponsored Fast-track Young Scientist (SR/FTP/PS-188/2012). We thank the anonymous referee of this paper for very detailed and useful comments, which helped in improving the quality of the paper.

REFERENCES

Belloni, T., Homan, J., Casella, P., et al., 2005, A&A, 440, 207

Cambier, H. J., & Smith, D. M., 2013, ApJ, 767, 46

Capitanio, F., Belloni, T., & Del Santo, M., et al., 2009, MNRAS, 398, 1194 - 1200

Chakrabarti, S.K., 1989, MNRAS, 240, 7

Chakrabarti, S. K., 1990a, "Theory of Transonic Astrophysical Flows", World Scientific (Singapore)

Chakrabarti, S. K., 1990b, ApJ, 362, 406

Chakrabarti, S. K., Molteni, D., 1995, MNRAS, 272, 80

Chakrabarti, S.K., & Titarchuk, L.G., 1995, ApJ, 455, 623 (CT95)

Chakrabarti, S.K., & Molteni, D., 1995, MNRAS, 272, 80

Chakrabarti, S. K., 1996, ApJ, 464, 664

Chakrabarti, S.K., 1997, ApJ, 484, 313

Chkarabart, S.K., & Manickam, S.G., 2000, ApJ, 531, L41

Chakrabarti, S.K., Nandi, A., Debnath, D., Sarkar, R., & Dutta, B.G., 2005, IJP, 78, 841 (arXiv:astro-ph/0508024)

Chakrabarti, S.K., Debnath, D., Nandi, A., Pal, P.S., 2008, A&A, 498, L41

Chakrabarti, S.K., Mondal, S. & Debnath, D., 2015, MNRAS, 452, 3451 (CMD15)

Chatterjee, D., Debnath, D., Chakrabarti, S.K., Mondal, S., & Jana, A., 2016, ApJ, 827, 88

Debnath, D., Chakrabarti, S.K., Nandi, A., & Mandal, S., 2008, BASI, 36, 151

Debnath, D., Chakrabarti, S.K., & Nandi, A., 2010, A&A, 520, 98

Debnath, D., Chakrabarti, S.K., & Nandi, A., 2013, AdSpR, 52, 2143

Debnath, D., Mondal, S., & Chakrabarti, S.K., 2014, MNRAS, 440, L121

Debnath, D., Mondal, S., & Chakrabarti, S.K., 2015a, MNRAS, 447, 1984

Debnath, D., Molla, A. A., Chakrabarti, S. K., & Mondal, S., 2015b, ApJ, 803, 59

Dewangan, G. C., Titarchuk, L., & Griffiths, R. E., 2006, ApJ, 637, L21

Doxsey, R., Bradt, H., Fabbiano, G., et. al., 1977, IAU Circ., 3113, 2

Emelyanov, A. N., Aleksandrovich, N. L., & Sunyaev, R. A., 2000, AstL, 26, L297

Farinelli, R., Titarchuk, L., Paizis, A., Frontera, F., 2008, ApJ, 680, 620

Fiorito, R., & Titarchuk, L.G., 2004, ApJ, 614, L113

Galeev, A.A., Rosner, R., & Vaiana, G.S., 1979, ApJ, 229, 318

Giri, K., & Chakrabarti, S.K., 2013, MNRAS, 430, 2836

Giacche, S., Gilli, R., & Titarchuk, L., A&A, 2014, 562, 44

Greene, J., Bailyn, C.D., & Orosz, J. A., 2001, ApJ, 554, 1290

Gursky, H., Bradt, H., Doxsey, R., et al., 1978, ApJ, 223, 973

Haardt, F., & Maraschi, L., 1993, ApJ, 413, 507

Jana, A., Debnath, D., & Chakrabarti, S. K., et al., 2016, ApJ, 819, 107

Kaluzienski, L. J., & Holt, S. S., 1997, IAU Circ., 3099, 3

Kuulkers, E., Chenevez, J., & Altamirano, D., et al., 2011, ATel, 3263, 1

Markwardt, C. B., & Swank, J. H., 2003, ATel, 133, 1

McClintock, J. E., & Remillard, R. A., 2006, in Compact Stellar X-ray Sources, Cambridge, Astrophysical Ser., vol. 39, ed. W. Lewin & M. van der Klis (Cambridge Univ. Press), 157

McClintock, J. E., Remillard, R. A., Rupen, M. P., Torres, M. A. P., Steeghs, D., Levine, A. M., & Orosz, J. A. 2009, ApJ, 698, 1398

Molteni, D., Sponholz, H., & Chakrabarti, S.K., 1996, ApJ, 457, 805

Molla, A. A., Debnath, D., Chakrabarti, S. K., Mondal, S., Jana, A., 2016, MNRAS, 460, 3163

Mondal, S., & Chakrabarti, S.K., 2013, MNRAS, 431, 2716

Mondal, S., Debnath, D., & Chakrabarti, S.K., 2014, ApJ, 786, 4

Mondal, S., Chakrabarti, S.K., & Debnath, D., 2014, Ap&SS, 353, 223

Mondal, S., Chakrabarti, S.K., & Debnath, D., 2015, ApJ, 798, 57

Mondal, S., Chakrabarti, S.K., & Debnath, D., 2016, Ap&SS, 361, 309

Nandi, A., Debnath, D., Mandal, S., & Chakrabarti, S.K., 2012, A&A, 542, 56

Papadakis, I. E., Sobolewska, M., Arevalo, P., et al., 2009, A&A, 494, 905

Petri, J., 2008, Ap&SS, 318, 181

Raynolds, P. S., 1999, ApL&C, 38, 425

Remillard, R.A., & McClintock, J.E., 2006, A&A, 44, 49

Revnivstev, M., CheRNyakova, M., Capitanio, F., et al., 2003, ATel, 132, 1

Seifina, E., Titarchuk, L., Shaposhnikov, N., 2014, ApJ, 789, 57

Shakura, N.I., & Sunyaev, R.A., 1973, A&A, 24, 337

Shaposhnikov, Ni, & Titarchuk, L., 2007, ApJ, 663, 445 (ST07)

Shaposhnikov, Ni, & Titarchuk, L.G., 2009, ApJ, 699, 453 (ST09)

Smith, D., Heindl, W.A., & Swank, J.H., 2002, ApJ, 569, 362

Sobolewska, M. A., & Papadakis, I. E., 2009, MNRAS, 399, 1997

Soria, R., Wu, K., & Hannikainen, D., et al., 2001, Proc. of workshop on "X-Ray emission from Accretion onto Black Holes", 65

Steiner, J. F., McClintock, J. E., & Reid, M. J., 2012, ApJL, 745, L7

Strohmayer, T. E., Mushotzky, R., Winter, L., Soria, R., Uttley, P., & Cropper, M., 2007, ApJ, 660, 580

Sunyaev, R.A., & Titarchuk, L.G., 1980, ApJ, 86, 121

Sunyaev, R.A., & Titarchuk, L.G., 1985, A&A, 143, 374

Titarchuk, L.G., & Fiorito, R., 2004, ApJ, 612, 988

Titarchuk, L.G., & Seifina, E., 2016a, A & A, 585, 94

Titarchuk, L.G., & Seifina, E., 2016b, A & A, in press (astro-ph/160900780)

Titarchuk, L.G., & Wood, K., 2002, ApJ, 612, 988

Tomsick, J. A., Yamaoka, K., & Stephane, C., et al., 2014, ApJ, 791, 70

Wu, K. et al., 2002, ApJ, 565, 1161

Yamaoka, K., Negoro, H., & Sugizaki, M., et al., 2010, ATel, 2378, 1

Zdziarski, A.A., Lubinski, P., & Gilfanov, M., et al., 2003, MNRAS, 342, 355

This 2-column preprint was prepared with the AAS LaTeX macros v5.2.

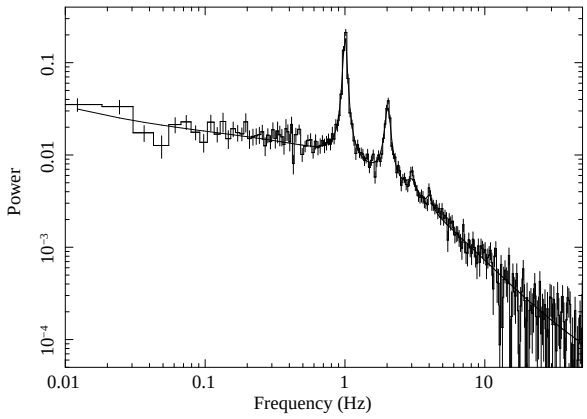

Fig. 1.— Power density spectrum of 0.01 sec time binned PCU2 light curve in the energy of 2 – 15 keV with an exposure time of 3379s is shown for the observation Id 95360-14-01-00 (MJD=55418.43) of 2010 outburst. It has been fitted with combination of five Lorentzians (one broad for initial break part and others for four QPO peaks) and one power-law (for late slope) models. The frequency of the primary dominating QPO is found to be 1.008 ± 0.003 Hz.

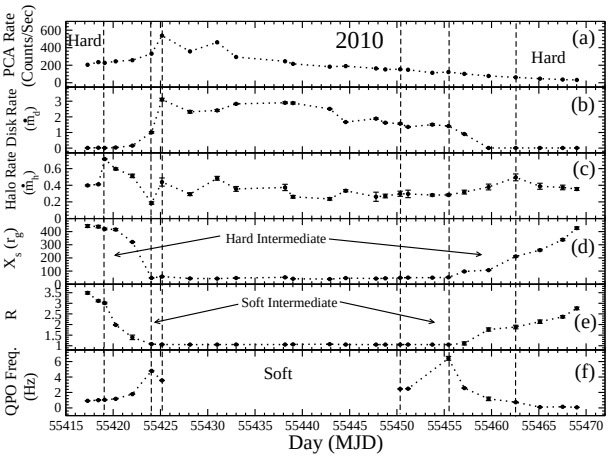

Fig. 2.— Variation of (a) 2.5 – 25 keV PCA count rates (cnts/sec), (b) TCAF fitted disk (accretion) rate $\dot{m}_d$ in $\dot{M}_{Edd}$ unit, (c) sub-Keplerian halo $\dot{m}_h$ rate in $\dot{M}_{Edd}$ unit, and (d) TCAF fitted shock location (X_s) in $2GM/c^2$ unit, (e) strength of the shock (R), in the 2.5 – 25 keV energy band keeping an average normalization constant of N = 15.55. Along the X-axis is the observation day (MJD) for the 2010 outburst. In (f), the observed primary dominating QPO frequencies (in Hz) with day (MJD) are shown. The vertical dashed lines indicate transitions between different spectral states.

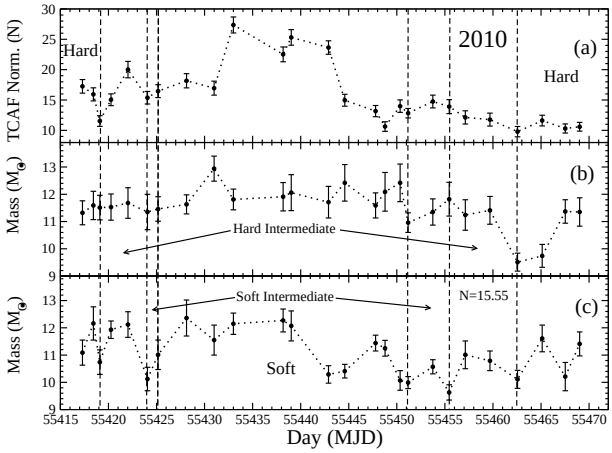

Fig. 3.— Variations of TCAF model fitted parameters: (a) normalization, and (b) mass of the black hole (M_{BH} in $M_\odot$) over the entire period of the 2010 outburst of H 1743-322 are shown when all model parameters are kept as free. In (c), TCAF fitted M_{BH} values are shown when model normalization was kept frozen at 15.55, which we get by taking the weighted average of the normalization values of panel (a).

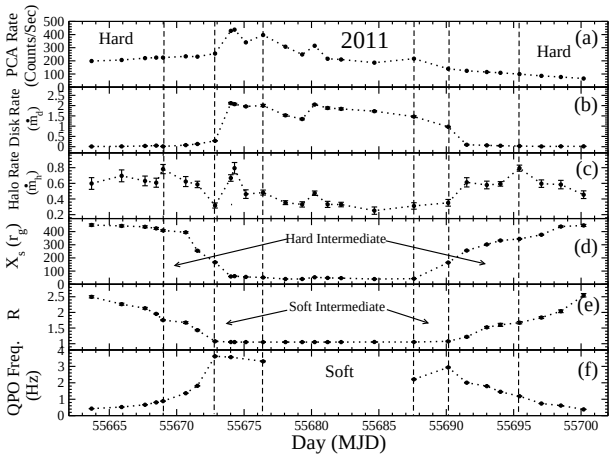

Fig. 4.— Same as Fig. 2, except for 2011 outburst H 1743-322

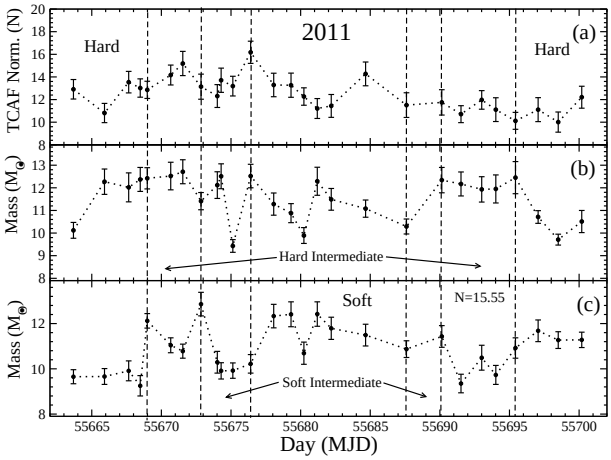

Fig. 5.— Same as Fig. 3, except for 2011 outburst of H 1743-322.

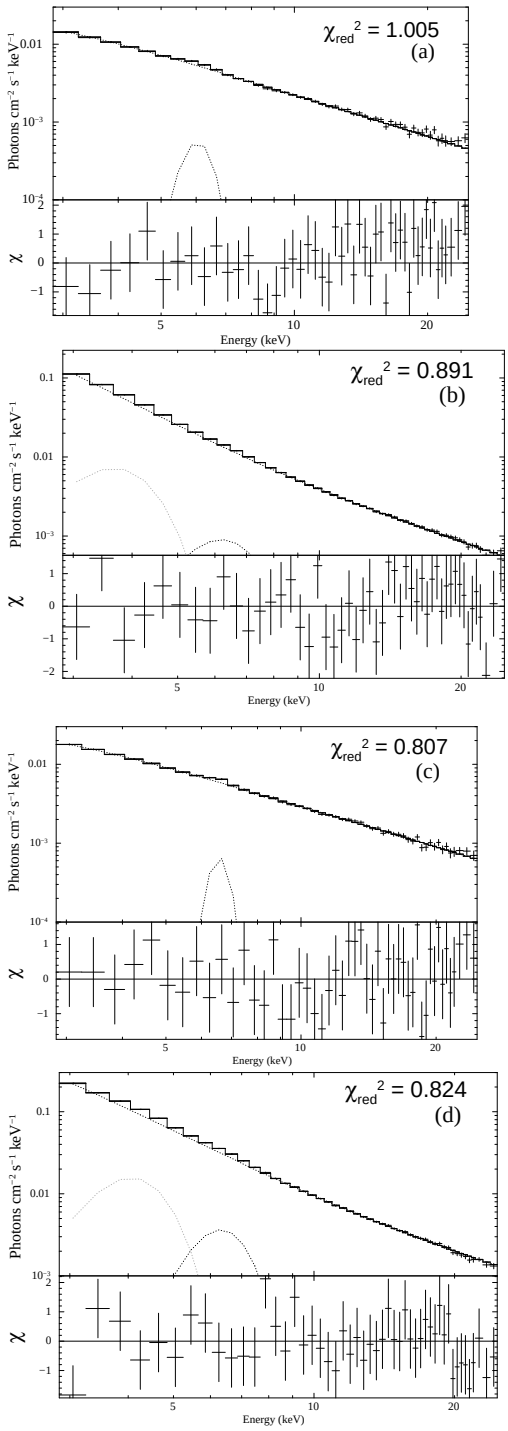

Fig. 6.— TCAF model fitted unfolded spectrum for (a) hard state (Obs Id: 95360-14-25-01), (b) soft state (Obs Id: 95360-14-15-00) from 2010 outburst of H 1743-322 are shown. Same for (c) hard state (Obs Id: 96425-01-06-02), (d) soft state (Obs Id: 96425-01-03-00) from 2011 outburst of H 1743-322 are shown. For a constant normalization, better fits, especially in softer states require double Gaussians having peaks at around 3.8 keV and 6.5 keV respectively with the normalization of the first component increasing with photon index. See text for details.

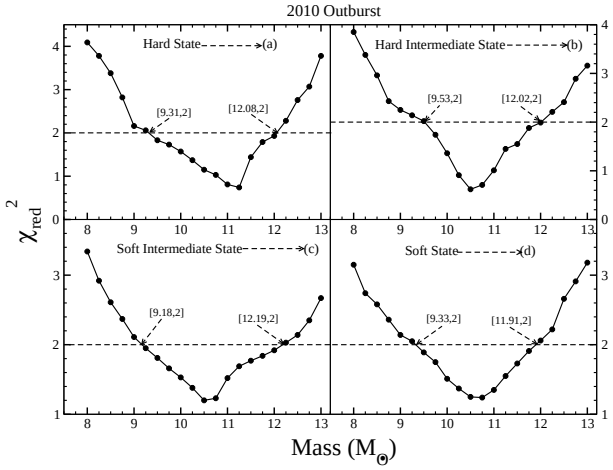

Fig. 7.— (a)-(d) variation of χ^2_{red} with mass of the black hole in solar mass($M_\odot$) unit for four different observations selected from four spectral states HS, HIMS, SIMS and SS for 2010 outburst. Here the square brackets denotes the value of mass for acceptable reduced χ^2 limit (≤ 2.0) .

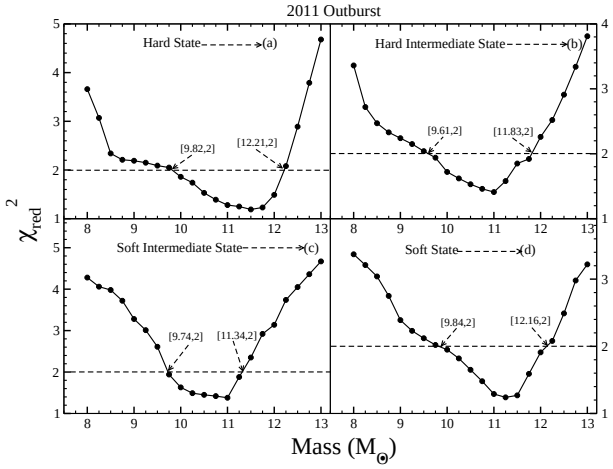

Fig. 8.— Same as Fig. 7, except for 2011 outburst of H 1743-322

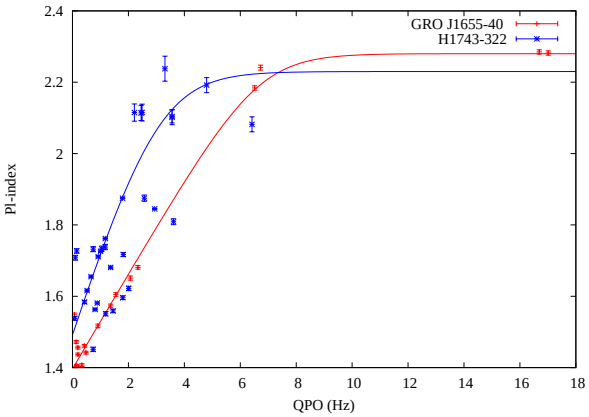

Fig. 9.— Photon index - QPO frequency correlations data for H 1743-322 for 2010 & 2011 outbursts (online blue points) and GRO J1655-40 during the 2005 outburst data (online red points). The data are fitted with a model function to apply a scaling method. We obtain the BH mass H 1743-322 in the range of $11.65 \pm 0.67 M_\odot$ using the scaling method and the well-known BH mass of GRO J1655-40, which is in the range of $6.3 \pm 0.5 M_\odot$. The result is obtained by using model composition wabs×(CompTB+Gaussian).

Appendix Table I

TCAF Model Fitted parameters during 2010 outburst

Obs.	Id	Day (MJD)	$\dot{m}_d$ ($\dot{M}_{Edd}$)	$\dot{m}_h$ ($\dot{M}_{Edd}$)	X_S r_g	R	$ga1$ (keV)	$sigma1$ (keV)	$norm1$ $*10^{-3}$	$ga2$ (keV)	$sigma2$ (keV)	$norm2$ $*10^{-3}$	QPO (Hz)	χ^2_{red}(dof)
(1)	(2)	(3)	(4)	(5)	(6)	(7)	(8)	(9)	(10)	(11)	(12)	(13)	(14)	(15)
1	X-01-00	55417.3	$0.013^{\pm0.005}$	$0.398^{\pm0.007}$	$442.1^{\pm10.6}$	$3.491^{\pm0.056}$	$6.31^{\pm0.26}$	$0.65^{\pm0.15}$	$2.9^{\pm0.8}$	$3.83^{\pm0.21}$	$0.79^{\pm0.25}$	$4.58^{\pm1.11}$	$0.919^{\pm0.004}$	1.09(39)
2	Y-01-00	55418.4	$0.025^{\pm0.009}$	$0.411^{\pm0.005}$	$437.7^{\pm9.3}$	$3.117^{\pm0.045}$	$6.39^{\pm0.31}$	$0.58^{\pm0.21}$	$2.5^{\pm0.6}$	$3.89^{\pm0.25}$	$0.81^{\pm0.18}$	$4.21^{\pm1.32}$	$1.008^{\pm0.003}$	0.76(39)
3	Y-02-01	55419.1	$0.011^{\pm0.005}$	$0.715^{\pm0.007}$	$419.7^{\pm6.3}$	$3.012^{\pm0.039}$	$6.22^{\pm0.38}$	$0.81^{\pm0.24}$	$4.8^{\pm1.2}$	$3.59^{\pm0.17}$	$0.76^{\pm0.23}$	$7.91^{\pm1.55}$	$1.045^{\pm0.008}$	1.51(39)
4	Y-02-00	55420.3	$0.039^{\pm0.011}$	$0.597^{\pm0.011}$	$415.6^{\pm7.9}$	$1.981^{\pm0.015}$	$6.22^{\pm0.35}$	$0.75^{\pm0.14}$	$3.7^{\pm0.8}$	$3.66^{\pm0.38}$	$0.82^{\pm0.13}$	$6.11^{\pm1.75}$	$1.174^{\pm0.002}$	1.26(39)
5	Y-02-03	55422.0	$0.158^{\pm0.019}$	$0.612^{\pm0.021}$	$320.9^{\pm3.1}$	$1.394^{\pm0.107}$	$6.54^{\pm0.45}$	$0.31^{\pm0.09}$	$2.1^{\pm0.9}$	$4.42^{\pm0.42}$	$0.35^{\pm0.11}$	$2.08^{\pm1.12}$	$1.789^{\pm0.017}$	0.68(39)
6	Y-03-01	55424.1	$1.008^{\pm0.051}$	$0.186^{\pm0.015}$	$47.6^{\pm1.2}$	$1.075^{\pm0.015}$	$6.13^{\pm0.32}$	$0.75^{\pm0.16}$	$5.6^{\pm1.6}$	$3.35^{\pm0.35}$	$0.65^{\pm0.21}$	$29.1^{\pm5.4}$	$4.796^{\pm0.022}$	1.19 (39)
7	Y-04-00	55425.2	$3.105^{\pm0.084}$	$0.439^{\pm0.049}$	$58.3^{\pm2.2}$	$1.058^{\pm0.013}$	$6.08^{\pm0.18}$	$0.92^{\pm0.13}$	$17.1^{\pm2.3}$	$3.91^{\pm0.49}$	$0.81^{\pm0.15}$	$64.7^{\pm8.6}$	$3.558^{\pm0.024}$	1.39(39)
8	Y-05-00	55428.1	$2.324^{\pm0.085}$	$0.273^{\pm0.017}$	$43.8^{\pm1.5}$	$1.053^{\pm0.005}$	$6.16^{\pm0.29}$	$0.95^{\pm0.12}$	$9.2^{\pm1.6}$	$3.85^{\pm0.72}$	$0.81^{\pm0.28}$	$57.9^{\pm9.8}$	* * * * *	1.33(39)
9	Y-07-00	55431.1	$2.412^{\pm0.058}$	$0.484^{\pm0.023}$	$42.8^{\pm1.2}$	$1.053^{\pm0.004}$	$6.37^{\pm0.39}$	$0.71^{\pm0.11}$	$6.7^{\pm1.9}$	$3.98^{\pm0.47}$	$0.77^{\pm0.25}$	$42.4^{\pm7.8}$	* * * * *	1.39(39)
10	Y-06-01	55433.1	$2.831^{\pm0.033}$	$0.356^{\pm0.029}$	$47.2^{\pm0.9}$	$1.054^{\pm0.005}$	$6.29^{\pm0.45}$	$0.55^{\pm0.15}$	$5.4^{\pm1.4}$	$3.31^{\pm0.32}$	$0.88^{\pm0.21}$	$84.2^{\pm5.1}$	* * * * *	0.67(39)
11	Y-10-00	55438.2	$2.902^{\pm0.058}$	$0.374^{\pm0.038}$	$52.5^{\pm1.5}$	$1.054^{\pm0.004}$	$6.21^{\pm0.29}$	$0.81^{\pm0.24}$	$3.3^{\pm0.6}$	$3.62^{\pm0.46}$	$0.74^{\pm0.32}$	$40.6^{\pm8.4}$	* * * * *	0.87(39)
12	Y-11-00	55439.1	$2.881^{\pm0.061}$	$0.261^{\pm0.016}$	$41.5^{\pm0.7}$	$1.062^{\pm0.004}$	$6.11^{\pm0.34}$	$0.71^{\pm0.19}$	$4.0^{\pm1.1}$	$3.15^{\pm0.23}$	$0.95^{\pm0.08}$	$101^{\pm21}$	* * * * *	0.92(39)
13	Y-13-00	55442.9	$2.508^{\pm0.028}$	$0.236^{\pm0.015}$	$39.1^{\pm0.7}$	$1.071^{\pm0.005}$	$5.91^{\pm0.44}$	$0.98^{\pm0.07}$	$4.4^{\pm1.7}$	$3.32^{\pm0.36}$	$0.88^{\pm0.14}$	$63.7^{\pm9.8}$	* * * * *	1.25(39)
14	Y-15-00	55444.6	$1.668^{\pm0.019}$	$0.334^{\pm0.013}$	$46.9^{\pm0.6}$	$1.055^{\pm0.003}$	$6.21^{\pm0.41}$	$0.91^{\pm0.09}$	$2.2^{\pm0.8}$	$3.62^{\pm0.55}$	$0.69^{\pm0.24}$	$14.5^{\pm3.5}$	* * * * *	0.89(39)
15	Y-18-00	55447.8	$1.885^{\pm0.048}$	$0.262^{\pm0.055}$	$43.2^{\pm0.6}$	$1.053^{\pm0.002}$	$6.22^{\pm0.45}$	$0.75^{\pm0.15}$	$2.1^{\pm0.7}$	$3.38^{\pm0.18}$	$0.78^{\pm0.32}$	$19.7^{\pm4.8}$	* * * * *	1.14(39)
16	Y-19-00	55448.8	$1.623^{\pm0.022}$	$0.271^{\pm0.048}$	$44.9^{\pm0.8}$	$1.052^{\pm0.004}$	$6.21^{\pm0.43}$	$0.85^{\pm0.13}$	$1.6^{\pm0.5}$	$3.21^{\pm0.23}$	$0.42^{\pm0.21}$	$27.1^{\pm5.4}$	* * * * *	0.95(39)
17	Y-20-00	55450.3	$1.564^{\pm0.041}$	$0.298^{\pm0.031}$	$49.1^{\pm0.9}$	$1.053^{\pm0.003}$	$6.62^{\pm0.51}$	$0.75^{\pm0.31}$	$2.8^{\pm0.9}$	$4.19^{\pm0.39}$	$0.32^{\pm0.16}$	$1.33^{\pm0.45}$	$2.454^{\pm0.022}$	0.61(39)
18	Y-20-01	55451.2	$1.355^{\pm0.025}$	$0.296^{\pm0.045}$	$50.2^{\pm1.1}$	$1.054^{\pm0.003}$	$6.39^{\pm0.48}$	$0.85^{\pm0.35}$	$2.9^{\pm0.9}$	$3.73^{\pm0.33}$	$0.63^{\pm0.21}$	$4.12^{\pm1.11}$	$2.489^{\pm0.018}$	0.59(39)
19	Y-21-01	55453.7	$1.503^{\pm0.055}$	$0.282^{\pm0.012}$	$49.9^{\pm1.1}$	$1.052^{\pm0.004}$	$6.51^{\pm0.45}$	$0.31^{\pm0.11}$	$0.3^{\pm0.1}$	$3.18^{\pm0.22}$	$0.59^{\pm0.34}$	$11.8^{\pm2.1}$	* * * * *	0.81(39)
20	Y-22-01	55455.4	$1.408^{\pm0.019}$	$0.284^{\pm0.011}$	$52.5^{\pm1.9}$	$1.053^{\pm0.003}$	$6.71^{\pm0.52}$	$0.71^{\pm0.18}$	$2.1^{\pm0.8}$	$4.44^{\pm0.56}$	$0.31^{\pm0.14}$	$0.27^{\pm0.07}$	$6.417^{\pm0.252}$	0.86(39)
21	Y-23-01	55457.1	$0.041^{\pm0.009}$	$0.311^{\pm0.025}$	$96.1^{\pm2.2}$	$1.136^{\pm0.085}$	$6.56^{\pm0.62}$	$0.33^{\pm0.16}$	$0.1^{\pm0.1}$	– – – –	– – – –	– – – –	$2.569^{\pm0.044}$	1.09(42)
22	Y-24-01	55459.7	$0.011^{\pm0.005}$	$0.379^{\pm0.035}$	$107.3^{\pm3.1}$	$1.764^{\pm0.077}$	$6.37^{\pm0.12}$	$0.32^{\pm0.08}$	$0.2^{\pm0.1}$	– – – –	– – – –	– – – –	$1.172^{\pm0.226}$	1.31(42)
23	Y-25-01	55462.6	$0.010^{\pm0.005}$	$0.495^{\pm0.041}$	$211.3^{\pm4.9}$	$1.882^{\pm0.085}$	$6.04^{\pm0.14}$	$0.42^{\pm0.22}$	$0.1^{\pm0.1}$	– – – –	– – – –	– – – –	$0.741^{\pm0.046}$	1.01(42)
24	Y-28-00	55465.1	$0.011^{\pm0.004}$	$0.388^{\pm0.036}$	$259.3^{\pm5.9}$	$2.134^{\pm0.082}$	$6.63^{\pm0.55}$	$0.33^{\pm0.18}$	$0.3^{\pm0.1}$	– – – –	– – – –	– – – –	$0.102^{\pm0.003}$	1.24(42)
25	Y-26-02	55467.5	$0.010^{\pm0.005}$	$0.374^{\pm0.028}$	$338.3^{\pm7.7}$	$2.365^{\pm0.055}$	$6.42^{\pm0.41}$	$0.35^{\pm0.09}$	$0.1^{\pm0.1}$	– – – –	– – – –	– – – –	$0.149^{\pm0.005}$	1.02(42)
26	Y-28-01	55469.0	$0.011^{\pm0.004}$	$0.355^{\pm0.017}$	$426.6^{\pm9.2}$	$2.762^{\pm0.062}$	$6.41^{\pm0.29}$	$0.74^{\pm0.17}$	$0.1^{\pm0.1}$	– – – –	– – – –	– – – –	$0.079^{\pm0.002}$	1.11(42)

Here X=95368-01, Y=95360-14 are the initial part of observation IDs. In Columns 4, 5, 6 & 7 we show TCAF model fitted disk rate ($\dot{m}_d$), halo rate ($\dot{m}_h$), shock location (X_s) and shock compression ratio (R) along with their error bars during the 2010 outburst. In Columns 8,9,10,11,12 & 13 we show Gaussian line energy, sigma and normalization for two Gaussian used to fit the spectra of the BH In Columns 14 & 15 we present observed QPO values and value of χ^2_{red} with no. of degrees of freedom mentioned in the brackets. The "err" command is used to find 90% confidence ± error values for the model fitted parameters. The result is obtained by using model composition wabs*(TCAF+Gaussian+Gaussian).

Appendix Table II

TCAF Model Fitted parameters during 2011 outburst

Obs.	Id	Day	$\dot{m}_d$	$\dot{m}_h$	X_S	R	$ga1$	$sigma1$	$norm1$	$ga2$	$sigma2$	$norm2$	QPO	χ^2_{red}(dof)
		(MJD)	($\dot{M}_{Edd}$)	($\dot{M}_{Edd}$)	r_g		(keV)	(keV)	$*10^{-3}$	(keV)	(keV)	$*10^{-3}$	(Hz)	
(1)	(2)	(3)	(4)	(5)	(6)	(7)	(8)	(9)	(10)	(11)	(12)	(13)	(14)	(15)
1	Z-01-00	55663.7	$0.010^{\pm0.005}$	$0.598^{\pm0.075}$	$449.9^{\pm8.8}$	$2.498^{\pm0.035}$	$6.41^{\pm0.36}$	$0.47^{\pm0.22}$	$2.1^{\pm0.97}$	$4.02^{\pm0.29}$	$0.77^{\pm0.34}$	$3.9^{\pm1.3}$	$0.428^{\pm0.001}$	0.91(39)
2	Z-01-01	55665.9	$0.013^{\pm0.007}$	$0.696^{\pm0.076}$	$443.1^{\pm7.7}$	$2.263^{\pm0.032}$	$6.18^{\pm0.29}$	$0.61^{\pm0.27}$	$2.7^{\pm1.1}$	$3.54^{\pm0.35}$	$0.98^{\pm0.08}$	$7.8^{\pm2.2}$	$0.524^{\pm0.002}$	1.49(39)
3	Z-02-00	55667.7	$0.035^{\pm0.008}$	$0.631^{\pm0.062}$	$436.1^{\pm7.6}$	$2.132^{\pm0.029}$	$6.21^{\pm0.22}$	$0.83^{\pm0.11}$	$3.6^{\pm1.2}$	$3.58^{\pm0.32}$	$0.68^{\pm0.21}$	$5.6^{\pm2.4}$	$0.664^{\pm0.002}$	1.25(39)
4	Z-02-04	55668.5	$0.053^{\pm0.003}$	$0.608^{\pm0.058}$	$424.2^{\pm7.1}$	$1.953^{\pm0.015}$	$6.31^{\pm0.42}$	$0.61^{\pm0.26}$	$2.1^{\pm0.9}$	– – –	– – –	– – –	$0.807^{\pm0.003}$	1.39(42)
5	Z-02-01	55667.0	$0.013^{\pm0.008}$	$0.782^{\pm0.059}$	$408.5^{\pm5.9}$	$1.754^{\pm0.017}$	$6.26^{\pm0.45}$	$0.58^{\pm0.17}$	$2.1^{\pm0.8}$	– – –	– – –	– – –	$0.885^{\pm0.004}$	1.37(42)
6	Z-02-02	55670.7	$0.075^{\pm0.007}$	$0.623^{\pm0.064}$	$394.1^{\pm6.1}$	$1.675^{\pm0.028}$	$6.21^{\pm0.39}$	$0.68^{\pm0.31}$	$3.5^{\pm1.2}$	$3.51^{\pm0.19}$	$0.69^{\pm0.11}$	$5.9^{\pm2.3}$	$1.364^{\pm0.007}$	1.38(39)
7	Z-02-05	55671.5	$0.131^{\pm0.004}$	$0.586^{\pm0.041}$	$254.5^{\pm4.2}$	$1.433^{\pm0.021}$	$6.32^{\pm0.42}$	$0.74^{\pm0.22}$	$3.4^{\pm0.8}$	$3.55^{\pm0.32}$	$0.48^{\pm0.14}$	$4.7^{\pm1.6}$	$1.816^{\pm0.015}$	1.40(39)
8	Z-02-03	55672.9	$0.286^{\pm0.011}$	$0.317^{\pm0.033}$	$167.1^{\pm2.9}$	$1.076^{\pm0.011}$	$6.23^{\pm0.29}$	$0.72^{\pm0.24}$	$2.1^{\pm0.6}$	$3.33^{\pm0.32}$	$0.45^{\pm0.09}$	$10.8^{\pm3.3}$	$3.614^{\pm0.021}$	1.35(39)
9	Z-03-00	55674.0	$2.118^{\pm0.038}$	$0.668^{\pm0.042}$	$58.8^{\pm0.8}$	$1.053^{\pm0.009}$	$6.32^{\pm0.46}$	$0.81^{\pm0.12}$	$7.4^{\pm2.9}$	$4.03^{\pm0.41}$	$0.68^{\pm0.21}$	$31.1^{\pm0.1}$	$3.562^{\pm0.019}$	0.82(39)
10	Z-03-05	55674.3	$2.071^{\pm0.042}$	$0.794^{\pm0.072}$	$61.4^{\pm0.8}$	$1.051^{\pm0.007}$	$6.64^{\pm0.52}$	$0.75^{\pm0.18}$	$4.6^{\pm2.1}$	$3.89^{\pm0.49}$	$0.69^{\pm0.21}$	$30.4^{\pm0.1}$	* * * * *	1.09(39)
11	Z-03-01	55675.1	$1.961^{\pm0.021}$	$0.462^{\pm0.055}$	$55.6^{\pm0.7}$	$1.052^{\pm0.004}$	$6.11^{\pm0.53}$	$0.77^{\pm0.28}$	$5.1^{\pm1.9}$	$3.71^{\pm0.41}$	$0.75^{\pm0.29}$	$20.1^{\pm0.1}$	* * * * *	0.92(39)
12	Z-03-02	55676.4	$2.004^{\pm0.054}$	$0.482^{\pm0.032}$	$51.4^{\pm1.1}$	$1.051^{\pm0.008}$	$6.41^{\pm0.55}$	$0.76^{\pm0.11}$	$6.5^{\pm2.2}$	$3.85^{\pm0.32}$	$0.78^{\pm0.17}$	$40.2^{\pm0.2}$	$3.306^{\pm0.028}$	1.49(39)
13	Z-03-03	55678.1	$1.525^{\pm0.041}$	$0.353^{\pm0.025}$	$40.1^{\pm0.6}$	$1.052^{\pm0.006}$	$6.24^{\pm0.38}$	$0.55^{\pm0.08}$	$5.6^{\pm1.8}$	$3.55^{\pm0.29}$	$0.45^{\pm0.05}$	$50.1^{\pm0.1}$	* * * * *	1.09(39)
14	Z-03-04	55679.3	$1.345^{\pm0.039}$	$0.331^{\pm0.034}$	$39.9^{\pm0.7}$	$1.052^{\pm0.006}$	$6.02^{\pm0.56}$	$0.72^{\pm0.29}$	$2.8^{\pm0.8}$	$3.35^{\pm0.41}$	$0.65^{\pm0.15}$	$39.8^{\pm0.1}$	* * * * *	1.54(39)
15	Z-04-02	55680.2	$2.051^{\pm0.021}$	$0.474^{\pm0.028}$	$52.9^{\pm0.8}$	$1.051^{\pm0.009}$	$6.03^{\pm0.45}$	$0.78^{\pm0.33}$	$4.9^{\pm2.1}$	$3.79^{\pm0.39}$	$0.67^{\pm0.29}$	$30.2^{\pm0.2}$	* * * * *	1.52(39)
16	Z-04-00	55681.2	$1.882^{\pm0.052}$	$0.331^{\pm0.039}$	$48.1^{\pm0.7}$	$1.051^{\pm0.015}$	$6.05^{\pm0.51}$	$0.76^{\pm0.28}$	$2.7^{\pm0.7}$	$3.43^{\pm0.42}$	$0.54^{\pm0.19}$	$29.9^{\pm0.1}$	* * * * *	0.97(39)
17	Z-04-03	55682.2	$1.841^{\pm0.048}$	$0.329^{\pm0.029}$	$46.4^{\pm0.5}$	$1.052^{\pm0.005}$	$5.05^{\pm1.25}$	$0.58^{\pm0.31}$	$2.7^{\pm0.8}$	$3.41^{\pm0.45}$	$0.62^{\pm0.24}$	$31.1^{\pm0.1}$	* * * * *	0.98(39)
18	Z-04-01	55684.7	$1.728^{\pm0.032}$	$0.251^{\pm0.047}$	$39.5^{\pm0.7}$	$1.054^{\pm0.006}$	$6.23^{\pm0.45}$	$0.69^{\pm0.22}$	$2.3^{\pm0.5}$	$3.63^{\pm0.31}$	$0.68^{\pm0.23}$	$32.5^{\pm0.1}$	* * * * *	1.05(39)
19	Z-05-00	55687.6	$1.464^{\pm0.041}$	$0.311^{\pm0.041}$	$42.6^{\pm0.8}$	$1.053^{\pm0.009}$	$6.03^{\pm0.62}$	$0.95^{\pm0.02}$	$3.1^{\pm1.3}$	$3.85^{\pm0.39}$	$0.45^{\pm0.13}$	$6.1^{\pm2.4}$	$2.215^{\pm0.021}$	1.01(39)
20	Z-05-01	55690.1	$0.969^{\pm0.022}$	$0.351^{\pm0.043}$	$164.8^{\pm1.7}$	$1.076^{\pm0.014}$	$6.59^{\pm0.26}$	$0.33^{\pm0.11}$	$4.2^{\pm10.2}$	– – –	– – –	– – –	$2.936^{\pm0.024}$	1.57(42)
21	Z-05-02	55691.5	$0.094^{\pm0.021}$	$0.613^{\pm0.059}$	$255.9^{\pm2.9}$	$1.218^{\pm0.023}$	$6.36^{\pm0.37}$	$0.32^{\pm0.09}$	$47.6^{\pm8.3}$	– – –	– – –	– – –	$2.008^{\pm0.018}$	1.46(42)
22	Z-05-03	55693.0	$0.063^{\pm0.003}$	$0.579^{\pm0.049}$	$302.1^{\pm3.1}$	$1.523^{\pm0.027}$	$6.43^{\pm0.42}$	$0.41^{\pm0.07}$	$74.6^{\pm9.2}$	– – –	– – –	– – –	$1.798^{\pm0.012}$	1.21(42)
23	Z-06-00	55694.0	$0.046^{\pm0.006}$	$0.593^{\pm0.029}$	$332.2^{\pm3.8}$	$1.602^{\pm0.048}$	$6.71^{\pm0.48}$	$0.31^{\pm0.25}$	$36.4^{\pm6.5}$	– – –	– – –	– – –	$1.452^{\pm0.009}$	1.59(42)
24	Z-06-01	55695.4	$0.031^{\pm0.008}$	$0.794^{\pm0.033}$	$344.2^{\pm4.2}$	$1.672^{\pm0.042}$	$6.41^{\pm0.34}$	$0.73^{\pm0.27}$	$1.9^{\pm9.8}$	– – –	– – –	– – –	$1.186^{\pm0.007}$	1.16(42)
25	Z-06-02	55697.1	$0.012^{\pm0.009}$	$0.596^{\pm0.048}$	$375.9^{\pm4.4}$	$1.836^{\pm0.032}$	$6.57^{\pm0.28}$	$0.31^{\pm0.14}$	$55.8^{\pm6.8}$	– – –	– – –	– – –	$0.739^{\pm0.005}$	0.81(42)
26	Z-06-03	55698.5	$0.016^{\pm0.004}$	$0.584^{\pm0.054}$	$438.1^{\pm4.9}$	$2.037^{\pm0.043}$	$6.61^{\pm0.19}$	$0.35^{\pm0.16}$	$31.5^{\pm5.2}$	– – –	– – –	– – –	$0.614^{\pm0.003}$	1.01(42)
27	Z-06-04	55700.2	$0.017^{\pm0.005}$	$0.455^{\pm0.049}$	$446.5^{\pm7.8}$	$2.548^{\pm0.055}$	$6.68^{\pm0.16}$	$0.38^{\pm0.22}$	$24.1^{\pm4.6}$	– – –	– – –	– – –	$0.382^{\pm0.002}$	1.02(42)

Here, Z=96425-01 is the initial part of observation IDs. Footnotes are the same as Appendix Table I.

Appendix Table III

Table 1: TCAF Model Fitted Mass and Normalization Values during 2010 outburst

Obs.	Id	Day (MJD)	Normalization	Mass ($M_\odot$)	Mass ($M_\odot$)
1	95368-01-01-00	55417.3	$17.25^{\pm1.12}$	$11.32^{\pm0.44}$	$11.09^{\pm0.46}$
2	95360-14-01-00	55418.4	$15.93^{\pm1.08}$	$11.59^{\pm0.52}$	$12.16^{\pm0.61}$
3	95360-14-02-01	55419.1	$12.55^{\pm0.91}$	$11.08^{\pm0.48}$	$10.11^{\pm0.42}$
4	95360-14-02-00	55420.3	$15.04^{\pm0.97}$	$11.53^{\pm0.48}$	$11.93^{\pm0.32}$
5	95360-14-02-03	55422.0	$20.01^{\pm1.35}$	$11.68^{\pm0.56}$	$12.12^{\pm0.47}$
6	95360-14-03-01	55424.1	$15.37^{\pm1.03}$	$11.35^{\pm0.65}$	$10.12^{\pm0.43}$
7	95360-14-04-00	55425.2	$15.37^{\pm1.03}$	$12.21^{\pm0.52}$	$12.34^{\pm0.57}$
8	95360-14-05-00	55428.1	$19.21^{\pm1.13}$	$11.75^{\pm0.32}$	$11.91^{\pm0.69}$
9	95360-14-07-00	55431.1	$17.23^{\pm1.11}$	$11.32^{\pm0.42}$	$11.76^{\pm0.59}$
10	95360-14-06-01	55433.1	$27.36^{\pm1.32}$	$11.81^{\pm0.38}$	$12.15^{\pm0.39}$
11	95360-14-10-00	55438.2	$22.52^{\pm1.22}$	$11.91^{\pm0.52}$	$12.27^{\pm0.42}$
12	95360-14-11-00	55439.1	$25.31^{\pm1.28}$	$12.06^{\pm0.66}$	$12.07^{\pm0.55}$
13	95360-14-13-00	55442.9	$23.64^{\pm1.11}$	$11.71^{\pm0.58}$	$10.29^{\pm0.32}$
14	95360-14-15-00	55444.6	$14.96^{\pm0.98}$	$12.42^{\pm0.67}$	$10.41^{\pm0.25}$
15	95360-14-18-00	55447.8	$13.17^{\pm0.92}$	$11.59^{\pm0.46}$	$11.44^{\pm0.29}$
16	95360-14-19-00	55448.8	$10.63^{\pm0.79}$	$12.09^{\pm0.71}$	$11.25^{\pm0.29}$
17	95360-14-20-00	55450.3	$13.99^{\pm1.03}$	$12.42^{\pm0.69}$	$10.07^{\pm0.36}$
18	95360-14-20-01	55451.2	$12.83^{\pm0.78}$	$10.96^{\pm0.36}$	$9.99^{\pm0.22}$
19	95360-14-21-01	55453.7	$14.75^{\pm1.05}$	$11.35^{\pm0.48}$	$10.57^{\pm0.26}$
20	95360-14-22-01	55455.4	$13.91^{\pm1.15}$	$11.82^{\pm0.62}$	$9.63^{\pm0.28}$
21	95360-14-23-01	55457.1	$12.13^{\pm1.09}$	$11.24^{\pm0.56}$	$11.01^{\pm0.51}$
22	95360-14-24-01	55459.7	$11.77^{\pm1.07}$	$11.41^{\pm0.51}$	$10.79^{\pm0.36}$
23	95360-14-25-01	55462.6	$9.79^{\pm0.85}$	$9.51^{\pm0.33}$	$10.11^{\pm0.33}$
24	95360-14-28-00	55465.1	$11.61^{\pm0.88}$	$9.74^{\pm0.42}$	$11.61^{\pm0.49}$
25	95360-14-26-02	55467.5	$10.31^{\pm0.75}$	$11.37^{\pm0.43}$	$10.21^{\pm0.52}$
26	95360-14-28-01	55469.0	$10.59^{\pm0.72}$	$11.35^{\pm0.52}$	$11.41^{\pm0.44}$

In Columns 4 & 5 TCAF fitted model normalization and mass of the black hole are shown during 2010 outburst when all parameters during fitting are kept free, and in Column 6 model fitted mass is shown when normalization is frozen to 15.55.

Appendix Table IV

Table 2: TCAF Model Fitted Mass and Normalization Values during 2011 outburst

Obs.	Id	Day (MJD)	Normalization	Mass ($M_\odot$)	Mass ($M_\odot$)
1	96425-01-01-00	55663.7	$12.91^{\pm0.86}$	$10.12^{\pm0.35}$	$9.65^{\pm0.31}$
2	96425-01-01-01	55665.9	$10.81^{\pm0.85}$	$12.27^{\pm0.56}$	$9.66^{\pm0.35}$
3	96425-01-02-00	55667.7	$13.54^{\pm0.95}$	$12.02^{\pm0.64}$	$9.91^{\pm0.44}$
4	96425-01-02-04	55668.5	$13.02^{\pm0.81}$	$12.37^{\pm0.53}$	$9.25^{\pm0.45}$
5	96425-01-02-01	55667.0	$12.86^{\pm0.76}$	$12.42^{\pm0.47}$	$12.12^{\pm0.32}$
6	96425-01-02-02	55670.7	$14.17^{\pm0.88}$	$12.52^{\pm0.61}$	$11.04^{\pm0.33}$
7	96425-01-02-05	55671.5	$15.19^{\pm1.07}$	$12.71^{\pm0.53}$	$10.78^{\pm0.31}$
8	96425-01-02-03	55672.9	$13.14^{\pm1.11}$	$11.41^{\pm0.38}$	$12.86^{\pm0.52}$
9	96425-01-03-00	55674.0	$12.31^{\pm1.01}$	$12.12^{\pm0.59}$	$10.29^{\pm0.48}$
10	96425-01-03-05	55674.3	$13.71^{\pm1.07}$	$12.51^{\pm0.55}$	$9.91^{\pm0.36}$
11	96425-01-03-01	55675.1	$13.19^{\pm0.87}$	$9.43^{\pm0.28}$	$9.92^{\pm0.34}$
12	96425-01-03-02	55676.4	$16.18^{\pm0.98}$	$12.52^{\pm0.52}$	$10.22^{\pm0.41}$
13	96425-01-03-03	55678.1	$13.29^{\pm1.04}$	$11.28^{\pm0.49}$	$12.33^{\pm0.52}$
14	96425-01-03-04	55679.3	$13.27^{\pm1.07}$	$10.88^{\pm0.42}$	$12.41^{\pm0.55}$
15	96425-01-04-02	55680.2	$12.27^{\pm0.77}$	$9.89^{\pm0.35}$	$10.69^{\pm0.49}$
16	96425-01-04-00	55681.2	$11.21^{\pm0.88}$	$12.29^{\pm0.62}$	$12.42^{\pm0.54}$
17	96425-01-04-03	55682.2	$11.44^{\pm1.01}$	$11.49^{\pm0.48}$	$11.79^{\pm0.49}$
18	96425-01-04-01	55684.7	$14.27^{\pm1.05}$	$11.08^{\pm0.38}$	$11.49^{\pm0.48}$
19	96425-01-05-00	55687.6	$11.51^{\pm1.09}$	$10.29^{\pm0.33}$	$10.87^{\pm0.37}$
20	96425-01-05-01	55690.1	$11.75^{\pm1.12}$	$12.34^{\pm0.56}$	$11.43^{\pm0.48}$
21	96425-01-05-02	55691.5	$10.71^{\pm0.75}$	$12.17^{\pm0.53}$	$9.35^{\pm0.41}$
22	96425-01-05-03	55693.0	$11.97^{\pm0.82}$	$11.93^{\pm0.56}$	$10.49^{\pm0.55}$
23	96425-01-06-00	55694.0	$11.11^{\pm1.05}$	$11.95^{\pm0.62}$	$9.73^{\pm0.42}$
24	96425-01-06-01	55695.4	$10.12^{\pm0.75}$	$12.45^{\pm0.71}$	$10.92^{\pm0.45}$
25	96425-01-06-02	55697.1	$11.11^{\pm1.06}$	$10.71^{\pm0.28}$	$11.68^{\pm0.48}$
26	96425-01-06-03	55698.5	$10.01^{\pm0.89}$	$9.71^{\pm0.24}$	$11.27^{\pm0.37}$
27	96425-01-06-04	55700.2	$12.21^{\pm0.97}$	$10.51^{\pm0.49}$	$11.28^{\pm0.34}$

Footnotes are same as Appendix Table III